

**NASA TECHNICAL
TRANSLATION**



NASA TT F-697

C.1

NASA TT F-697

LOAN COPY: R
AFWL (D
KIRTLAND A



TO
1.

**PLASMA ACCELERATION IN A
TRAVELLING ELECTROMAGNETIC FIELD**
General Diagnostic and Velocity Measurements

by M. Charpenel, J. P. Rager, and B. Sitt

ONERA Tech. Note No. 174

Office National d'Études et de Recherches Aérospatiales

Châtillon, France, 1971

NATIONAL AERONAUTICS AND SPACE ADMINISTRATION • WASHINGTON, D. C. • SEPTEMBER 1971



0069046

NASA TT F-697

**PLASMA ACCELERATION IN A TRAVELLING
ELECTROMAGNETIC FIELD**

General Diagnostic and Velocity Measurements

By M. Charpenel, J. P. Rager, and B. Sitt

Translation of "Accélération d'un Plasma par un Champ
Électromagnétique Glissant. Diagnostics Généraux et
Mesures de Vitesse." ONERA Tech. Note No. 174,
Office National D'Études et de Recherches Aérospatiales,
Châtillon, France, 1971

NATIONAL AERONAUTICS AND SPACE ADMINISTRATION

For sale by the National Technical Information Service, Springfield, Virginia 22151
\$3.00

Table of Contents

	Page
Abstract	1
1 - Introduction	1
2 - Description of test set-up	3
2.1 - Description of accelerators	3
2.2 - Working-fluid supply unit-discharge control	5
3 - Diagnostic facilities - General characteristics of discharge plasma	6
3.1 - Introduction	6
3.2 - Direct measurements	6
3.2.1 - Flow-rate measurement	6
3.2.2 - Measurement of electric field and magnetic induction	8
3.2.3 - Measurement of ionization coefficient and mean electron temperature	8
3.2.4 - Determination of electron density	11
3.2.5 - Measurement of exhaust velocity	11
3.2.6 - Measurement of current density	15
3.3 - Indirect measurement of basic plasma parameters	17
3.3.1 - Principle	18
3.3.2 - Results	19
3.4 - Discussion	20
3.4.1 - Determination of ionization coefficient and of electron temperature and density	20
3.4.2 - Velocity measurements	21
3.4.3 - Interpretation of luminous phenomena	21
3.4.4 - Form of Ohm's law	23
Conclusion	26
References	28
List of captions	30

PLASMA ACCELERATION IN A TRAVELLING ELECTROMAGNETIC FIELD

General Diagnostic and Velocity Measurements

M. Charpenel, J.P. Rager, and B. Sitt

Office National d'Études et de Recherches Aéronautiques (ONERA), 92 Châtillon, France

Abstract

For the purpose of studying the processes of ionization and acceleration by travelling electromagnetic fields, and exploring the basic characteristics (temperature, density, velocity) of the plasma involved, an experimental device of pulsed operation has been created, which ensures simple diagnostic means for the measurement of electric and magnetic fields, induced current density, temperature and velocity. Another technique applied serves to determine the two last-named parameters indirectly. The results, when described and analysed, point to the presence, near the exit plane of the device, of a temperature wave propagating at the velocity of the relative electric field.

1 - Introduction

The interaction of an electromagnetic field with a conductive medium has been the seminal principle behind the design of many a device intended to convert electrical into kinetic energy. The advances made in aerospace research have promptly pointed the way to two prospective applications based on the use of a gaseous conductive medium namely in:

- a) accelerators for the propulsion of space probes or satellites;
- b) accelerators designed to produce jets of high stagnation enthalpies for

hypersonic wind tunnels.

It was by such vistas that the study of travelling-wave systems was originally inspired¹. It was not long before the research work carried out at ONERA in this field had thrown light on a still more fundamental benefit that might accrue from devices of this nature, in that they provide the experimenter with a dense plasma (approx. 10^{21} m^{-3}), which is fully ionized, chemically pure as ensured by the way it is produced (purely inductive self-ionization), and axisymmetric, thereby lending itself well to investigations into the physical properties of standard kinetic plasmas.

What are referred to as 'travelling-wave' devices can in broad terms be defined as inductive systems, with the applied electric and magnetic fields orthogonal, propagated with a determinate local phase velocity, and showing a spatial periodicity in the direction of propagation. Fluid ionization and acceleration are due to the action of these fields.

To explore the basic plasma characteristics (temperature, density, velocity) and the processes involved in acceleration by travelling electromagnetic fields, ONERA has evolved an experimental device of pulsed operation, which helps to hammer out straightforward diagnostic methods for the measurement of velocities, the induced current density and the electric and magnetic field.

This article describes the test set-up, outlines the diagnostic techniques evolved, and discusses their application to the determination of velocity, and of electron density and temperature, as derived from theoretical

considerations bearing on the equations of motion and of electron energy.

2 - Description of test set-up

In the light of the general objectives the foregoing research programme has set itself, a pulse-based mode of operation has on the whole been the obvious choice for a number of reasons, such as that :

- a) it permits the use of passive probes introduced into the flow as diagnostic aids;
- b) it disposes of some purely technological complications attendant on the construction of accelerators and their power sources, and irrelevant to the tasks in hand, thus making for a greatly simplified test equipment design.

2.1 - Description of accelerators

Certain theoretical considerations and performance test findings led Th. Moulin and J. Paulon ^{1, 5} to evolve accelerators with short divergent annular nozzles (Fig. 1), and with field velocities increasing from the throat to the exit plane. The factors weighed ^{2, 3, 4} include :

- i) the approx. 50 % limitation set on the theoretical efficiency in the event of a constant slip velocity of the electric field;
- ii) the non-homogeneous nature of the fluid along the centre-line channel, where it is subject to no force so long as the assembly carries no central body equipped with coils;
- iii) the marked drop in acceleration efficiency where the length of the accelerator is great in comparison with the spatial wavelength.

The electromagnetic configuration is made up by a set of windings fed

with two-phase current of medium frequency by a free-running oscillator : the discharge of two banks of capacitors of 0.75 μ F each, chargeable across 15,000 V, supplies the energizing currents, with the oscillator inductance provided, for each phase, by the corresponding coil of the accelerator.

The electric field induced is purely azimuthal; magnetic induction is largely radial in the middle of the channel. Their strength is attenuated in the direction of propagation so as to limit the effect of system distortions on the plasma motion. To prevent any coupling between phases, the coils are near-symmetrically arranged upstream and downstream of the nozzle throat.

The electric field strength is high enough to induce auto-ionization of the gas within the chosen range of working fluid flow rate. The phenomenon is of outstanding practical interest both for space applications and for investigations into the physics of plasma.

The following units have been designed on the model described above :

- a) two accelerators of the same length differing only in their radial dimensions (Fig. 2) and whose comparative investigation helps to ascertain any effect the channel height may have on operation;
- b) an accelerator with convergent-divergent annular nozzle, symmetrical about the throat; described at length in ⁶, it is intended to demonstrate the impact of magneto-hydrodynamic acceleration in certain conditions.

2.2 - Working-fluid supply unit-discharge control

The accelerator works in a vessel pre-evacuated to approx. 10^{-5} Torr, and is fed with working fluid (argon) by a twin-electrovalve system separating and then injecting a limited amount of gas (Fig. 3). The inlet valve opening pulse sets the starting instant of reference.

Figure 4 shows the subsequent variation pattern, as measured by a piezoelectric pick-up, of the static pressure prevailing on injection. The maximum pressure is proportional to the argon storage pressure (Fig. 5), so that once the latter has settled, the instantaneous flow rate varies solely with the time elapsed since the starting instant. In view of the extremely short accelerator running time (some tens of microseconds), as compared with the flow-rate variation time (a few milliseconds), (Fig. 6). The discharge can at this scale be regarded as instantaneous, and the flow rate as fully defined by the time-lag between the start pulse and the control pulse triggering the successive discharge, at a quarter-period interval, of the two banks of capacitors feeding each phase (Fig. 3).

The flow rate can thus be varied, at the moment of firing, by operating with two parameters, viz.

- a) current triggering delay;
- b) gas storage pressure.

It should, however, be noted that the choice of a high value for the time-lag, such as 3.5 m sec (corresponding to the peak of the flow rate vs. time curve), while ensuring optimum accuracy in determining the flow rate,

will at the same time result in setting up a counterpressure downstream of the accelerator, through an accumulation of gas expelled prior to the incoming of the currents and not at once exhausted by the pumps.

3 - Diagnostic facilities - General characteristics of discharge plasma

3.1 - Introduction

To define the characteristics of the type of plasma generated it is essential to know the orders of magnitude of the ionization coefficient, electron density and temperature, and velocity, as a means of determining the operation modes, and keeping track of their variations with the co-ordinates, with time, and with the system parameters (working-fluid flow rate, field strengths). Accurate measurements of electron density by microwave interferometer, and of electron temperature by spectrometry, entail recourse to sophisticated techniques, whose intricacy in use was at first out of all proportion to the objectives in view. Yet it was a simplified application of them which enabled the orders of magnitude to be worked out in numerical terms.

3.2 - Direct measurements

3.2.1 - Flow-rate measurement

The main difficulty in determining the mass flow rate of the cold gas fed to the accelerator lies in the largely unsteady pattern of this inflow. This 'snag' is got round by assuming the existence, at each instant, of a flow with a stagnation pressure yet to be determined, identical with the real flow, and amenable to the theory of isentropic steady flows. The sonic

throat condition for this imaginary flow will lead on to its stagnation pressure since this is proportional at any instant to the static pressure at the throat as embodied by the tube which connects the cavity enclosing the gas with the nozzle proper (Fig. 2). It has further been found that the variation with time of the static pressure in the gas shows a peak proportional in intensity to the pressure P_R in the tank (Fig. 5), and that the two curves plotted of tank pressures P_{R1} and P_{R2} derive from each other through an affinity of ratio P_{R1}/P_{R2} ; thus with P_R determined, this curve represents the variation of the fictitious stagnation pressure, as well as the flow rate, as a function of time. The order of magnitude of the flow rates so calculated is a few grammes per second for tank pressures lying close to the atmospheric and for a delay corresponding to the peak of the curve for static pressure at the throat.

These calculations and the underlying hypotheses have been checked by measuring :

- a) the static pressure and stagnation pressure at the nozzle exit;
 - b) the cold gas ejection velocity, using photomultipliers to determine the time-of-flight of a plasmoid produced by a discharge between two electrodes in the stream and entrained by the gas;
- and also by ascertaining that the integration of the flow rate/time curve results, in fact, in a mass of gas equal to that trapped between the two electrovalves.

3.2.2 - Measurement of electric field and magnetic induction

The azimuthal electric field E , with or without plasma, is determined by means of the potential difference arising at the ends of a circular conductive loop whose radius equals the channel mean radius; the electric field, at its maximum upon start of discharge (2000 to 3000 V.m^{-1}), shows a sinusoidal variation quasi-exponentially damped in time.

The radial magnetic field B is determined with the aid of a probe consisting of a single, 4 mm dia. loop suitable for local measurement, its normal arranged to lie along an accelerator diameter. Associated with it is a high-gain-valve or an R-C passive integrator. The maximum magnetic induction, of the order of 0.2 Tesla at the start of discharge, shapes up on much the same lines as the electric field.

3.2.3 - Measurement of ionization coefficient and mean electron temperature

A prism spectrograph is used for the spectral investigation, in the visible and the near UV range, of the light emitted by the plasma in the exit region during discharge, thus making for integration in space (over a plasma volume of some tens of cm^3) and especially in time, with about a hundred firings needed to make an image on the photoplate.

The spectrum obtained (Fig. 7 - a, b, c) is essentially a line spectrum, very rich in the ultraviolet, far less so in the visible range; its analysis mainly demonstrates excited states of the singly-ionized argon, and does not enable any particular line to be traced to the neutral argon with any certainty. This tends to infer full ionization of the plasma generated,

at any rate around the electron density peaks where emission is at its most intense.

An attempt has also been made to use this spectrum to measure electron temperature, on the assumption of local thermodynamic equilibrium, by determining relative line intensities. It should be borne in mind that an optically thin plasma (with no self-absorption in the medium) can be regarded as in local thermodynamic equilibrium as soon as there is high electron density (10^{21} m^{-3} or upwards) and low temperature (below 10^5 K), with the excitation and de-excitation process governed by collisions of electrons with heavy particles and the distribution function assumed to be Maxwellian⁷. To this case Boltzmann's law on the distribution of particles in various excited states is applicable, the intensity of a line of wavelength emitted by energy level E_m , is given by

$$(1) \quad I_{mn} = KN_0 \frac{g_m A_{mn}}{\lambda_{mn}} \exp - \frac{(E_m - E_0)}{kT_e}$$

where g_m is the statistical weight of the higher level, A_{mn} denotes the probability of transition from state m to state n , and k is a constant uniting the various geometric factors, N_0 stands for the heavy particles (in this particular case, singly-ionized argon atoms) in the fundamental state of energy E_0 .

In fact, the intensity of the spectral line recorded on the photographic plate corresponds to the time integration of this N_0/T_e function. As calculations have shown, in the event of periodic temperature variations

of fairly low relative amplitude (somewhere around 20 %), all it takes to obtain the integrated intensity is to substitute the mean for the instantaneous temperature and density values in the above expression.

With the experimental values of the ratio $\chi_m = I_{mn} \lambda_{mn} / g_m A_{mn}$ plotted in semi-logarithmic co-ordinates for different m values, as a function of the emission-level energy E_m , the result should be a straight line of a slope proportional to the reciprocal of the mean electron temperature T_e . The transition probabilities of the singly-ionized argon, required to compute χ_m , have been obtained from the oscillator strength s as determined by Griem⁷ in the LS-coupling approximation; the greater the line excitation energy, the closer this approximation. Regrettably enough, the spectrograph used had inadequate resolving power (angstrom order of magnitude) for the too closely spaced lines to be discriminated apart, leaving many of them susceptible of two alternative interpretations. Using the unequivocally identifiable ones alone, the points obtained give a mean straight line (Fig. 8). The method of least squares yields the most probable value of mean electron temperature, which has been found to be 17,000°K. The mean square error about this most probable value is 9 %.

It should be pointed out that, at this temperature, the Saha formula covering the ionization of argon on the local thermodynamic equilibrium hypothesis yields the following results for a 10^{21} m^{-3} density of singly-ionized argon:

$$\frac{n_+}{n_0} \approx 2.10^3 \quad \frac{n^{2+}}{n^+} \approx \frac{1}{2} \quad \frac{n^{3+}}{n^{2+}} \approx 10^{-3}$$

where n_0 is the density of neutral atoms, and n^+ , n^{2+} , n^{3+} those of singly, doubly and trebly ionized atoms. This calculation shows that a plasma of this kind only contains singly and doubly-ionized argon ions, which is consistent with the foregoing conclusion as to total ionization.

3.2.4 - Determination of electron density

Experience has shown that, in the particular flow-rate range (of the g/sec order), the plasma produced stops a microwave beam of 4 mm cutoff wavelength, corresponding to an electron density of over 6.10^{19} m^{-3} . Considering that the pre-firing density of neutral particles is approx. 8.10^{21} m^{-3} for a flow rate of 1 g/sec, this result enables the mean electron density to be estimated as lying between these two values.

A more accurate determination of this quantity, feasible with due allowance for the total ionization of the plasma, will be set forth in a later section, as it requires the exhaust velocity to be known as well.

3.2.5 - Measurement of exhaust velocity

The light phenomena attendant on plasma acceleration have been made amenable to analysis by the use of an ultra-high-speed camera. They involve a heavy modulation of a frequency twice that of the applied fields, and propagate in the direction of plasma ejection⁹.

This light emission was originally attributed to a continuous plasma background, and hence given the supposed form :

$$(2) \quad I \propto n_e^2 T_e^{-1/2}$$

I being the luminous intensity, and n_e and T_e the electron density and temperature of the plasma. The modulations of luminosity could at the line be conceived of as stemming largely from modulations of density prevailing over those of temperature. From the total plasma emitted light, as registered with the aid of photo-multipliers (lamps RCA EP 28, whose photo-sensitive film, type S 5, forms a pass-band over the approx. range of from 2,200 Å to 5,500 Å, with a well-defined sensitivity peak at 3400 Å), the velocity of propagation can be derived by measuring the time-of-flight between two planes near the exit section. Relevant tests yielded values ranging from 18.5 to 22 km.sec⁻¹, and pointed to no marked dependence on velocity as a function of the flow rate and of the intensity of the applied electromagnetic fields¹⁰. Since these values differed quite appreciably from the results of indirect measurement by the technique covered in 3.3, the assumptions underlying the direct method, and its mode of application, seemed to need revising in the light of these discrepancies, which may well mean that the travel of the light phenomena does not coincide with the motion of the plasma mass¹¹. The spectrographic examination has shown that the total light picked up by the photo-multipliers originates from the emission, not of a continuous background, but of a spectrum of ion lines. Thus, electron temperature enters exponentially into the intensity of light radiation (cf. formula 1), and the weak point in the foregoing method lies in the simultaneous dependence of this intensity on the parameters of both electron

temperature and electron density.

To exclude all temperature-responsive processes, there has been adopted a direct measurement method bound up with the mass motion of plasma. The 4 mm hyperfrequency emission cutoff caused by the passage of the plasma is solely dependent on electron density. Accordingly, by determining the time-of-flight of the cutoff steep front, the plasma exhaust velocity can be obtained.

Moreover, an experiment described in ⁶ has shown that the plasma produced by a geometrically as well as electromagnetically symmetric accelerator, working in a medium of argon at rest, turns up at one of the two accelerator ends only, notably at the one corresponding to the exit plane as defined by the direction of wave propagation. This rules out the hypothesis that attributes the observed cutoff to an ionization in situ of the injected gas, because such ionization is not seen to occur in the symmetrical plane (with respect to the throats) where the state of the electromagnetic field is the same. With the cutoff found to shift as far as something like 30 cm from the exit plane, where the applied fields no longer play any part, it is reasonable to infer that the displacement observed goes hand in hand with that of the plasma mass.

With the plasma-emitted light signals concurrently picked up at the same abscissae by means of photomultipliers, a comparison of the two recordings, coupled with determination of the propagation rates of the relative electric field and of the current density, will enable the observed displac-

ements to be evaluated. Figure 9 shows a typical oscillogram of the photomultiplier and hyperfrequency signals received. It reveals that the strong modulation recorded by the photomultipliers near the exit plane (Fig. 9 a) rapidly smoothes out when moving further and further away from it, only to leave a single peak close behind the cutoff (Fig. 9 b), both of which can be picked up at a considerable distance from the exit plane. The oscillation seen in Figure 9 b, following the cutoff of the diffraction of the signal received by the detector crystal represents the diffraction of the hyperfrequency beam on the upstream edge of the plasmoid .

Figures 10, 11, 12 and 13 offer a comprehensive view of the results for a flow rate of 1.2 g/sec. In ordinate the axial position of the photomultiplier/hyperfrequency-beam assembly is marked in with reference to an arbitrary origin. In abscissa are plotted the positions in time, as from the start of discharge, of the envelope vertex of the luminosity peaks supplied by the photomultipliers and of the cutoff front as indicated in Figure 9. One and the same figure conveys the respective data on the photomultipliers and the microwaves for equal values of the working parameters (charging voltage V of the banks of capacitors, current triggering delay τ , argon storage pressure H).

The tests performed lead to the following conclusions;

- a) the mean velocities obtained show no perceptible slowing down of the plasma over the distances covered;
- b) with the modulation of the luminosity signals in evidence, the travelling

speed of the cluster of peaks brought on by one particular firing is invariably something like 20 km. sec^{-1} . On the other hand, the vertex of their envelope moves at much the same speed as the single peak the signal contracts to on stoppage of modulation and as the cutoff front.

c) Exhaust velocity in the voltage range under consideration is barely affected by the initial charging voltage, i.e. the applied field strength, limited as it is by the equipment capabilities at the upper end of the range (18 kV) and by the occurrence of plasma instabilities at the lower end (8,5 kV).

d) The velocity falls off markedly (from approx. 7 to 10 km/sec in the cases shown in figures 10 and 11, down to anything like 3 km/sec as regards figures 12 and 13) if the counterpressure is increased at the accelerator exit while keeping the flow rate constant.

3.2.6 - Measurement of current density

The accelerator has a 'slip' regime, i.e., the plasma velocity is far lower than that of the travelling wave, resulting in a relatively strong induced current circulating in the plasma.

The measurement¹¹⁰ of this quantity is based on the use of small-size (average dia. 6 to 8 mm) Rogovski-type pick-up coils in conjunction with an R C passive integrator, directly providing the oscillogram of the current flowing through the probe. The probe may be of two types, viz.

- a) many-turn coil ($N \gg 100$) with insulating core;
- b) coil of few turns ($N \sim 20$) with iron-dust core.

Since all such probes are subject to a, sometimes appreciable, inductive

disturbance produced by the applied magnetic induction B, the double-layer winding scheme sets the coil elements in such opposing relative positions as to counteract the influence of that component of B which is normal to the probe plane. This still leaves that particular effect of the B component in the probe plane which is due to unevenness of the component over distances of the order of the probe size, and to irregularities in the winding. To neutralize this second spurious component calls for the use of a differential unit composed of the measuring probe and of a blind probe next to the former, which delivers the spurious signal alone (Fig. 14). Let it be noted that the use of a toroidal iron-dust core leaves the probe signal-to-noise ratio unaffected. As for the pass-band of the probe circuit, the influence of the inductance coil, which increases in proportion to μN^2 (μ being the magnetic permeability of iron dust), is decisive, and has led to the application of probes of type b).

In order to arrive at the current density, the useful cross section of the probe, or rather of the current tube flowing through and measured by it, must be determined. To this end, a checking procedure was carried out on a rail-type plasma gun¹², consisting in setting up an accurate chart of the effective magnetic-induction components and using it to compute the current density from the Maxwell equations, at various points of a grid. A registration of the values measured at these points by a Rogovski probe makes, by means of comparison, for a sequence of approximate values for the cross section sought, grouped about a mean value coming fairly close to the inner cross-section of the probe.¹⁵

Over the flow-rate range under investigation (from 0 to 6 g.sec⁻¹), the current density curve takes the shape plotted in figure 15. Its successive peaks are little affected by the value of this parameter at standard working rates of flow (Fig. 16), and b) the value of the current triggering delay at a given rate.

To try and account for the discrepancies in the results of the different velocity measurements, there have also been made time-of-flight measurements of the propagation velocity of current density peaks, between 0 and 30 mm from the accelerator exit, for charging voltages of 12 and 15 kV, for delays corresponding to the start (2.2 msec) and the peak (3.5 msec) of the injection pressure curve, and for flow-rate values ranging from approx. 1.6 g.sec⁻¹ to 8 g.sec⁻¹.

The mean propagation velocities of the various peaks over the distances explored are in the region of 20 km.sec⁻¹ (cf. the typical case illustrated in figure 17). The scatter in the measured values, which is of the same order as that occurring in the velocity measurements of the luminous phenomena, gives no indication whatsoever that the discharge parameters of delay, flow rate and charging voltage exert any influence.

3.3 - Indirect measurement of basic plasma parameters

Whenever applicable, indirect methods of determination can often be more flexible, even though less subtle in use than direct measurement. In this respect, the travelling-wave accelerator has been found to offer a versatile range of potential uses, and to enable the basic parameters of electron

temperature and density, and of velocity, to be arrived at through a measurement of subsidiary quantities, such as current density, and the electric and magnetic fields.

3.3.1 - Principle

Underlying the conception of the method is the possibility, afforded by the fully-ionized state of the gas, of applying Ohm's law to a binary plasma composed solely of electrons and just one kind of ions. With electron inertia disregarded, while due allowance is made for the lack of electrodes and the symmetry characteristics and overall neutrality of the plasma, the azimuthal projection of the equation of electron motion leads to the following relationship :

$$(3) \quad j = \sigma (E - uB)$$

where j is the azimuthal current density, u the axial velocity of the plasma and σ its scalar conductivity as defined, in particular, by Spitzer¹⁴, and having the form

$$(4) \quad \sigma = 7,8 \cdot 10^{-3} \frac{T_e^{3/2}}{\text{Log } \Lambda}$$

where

$$(5) \quad \Lambda = 12 \frac{(\epsilon_0 k T_e)^{3/2}}{n_e^{1/2} e^3}$$

ϵ_0 being the permittivity of vacuum, k Boltzmann's constant, and e the electron charge.

In view of the not negligible phase shift found between j , E and B , a concurrent measurement of these three quantities makes it possible to obtain

the plasma velocity u when $j = 0$ and the conductivity σ (hence the electron temperature) when $B = 0$. On the assumption that electron temperature varies with the relative electric field $(E - U B)$ alone, i.e., that the thermal-energy and pressure terms are negligible in the electron energy equation, the $\sigma(E)$ law coming into force whenever $B = 0$ may be extended to cover operation at instants of $B \neq 0$. This enables a complete temperature and velocity profile within a particular firing to be derived from the previous measurements^{11, 15}.

3.3.2 - Results

The measurements were performed with the aid of a triple probe (E, B, j). It was ascertained that the presence of the other two probes did not interfere with the response of either the electric-field or the current probe, and only slightly with that of the magnetic-field probe.

The set of data obtained derives from a test run in which the electric fields measured ranged from 0 to 600 V.m^{-1} .

The following findings were made :

a) For the whole set of test points (Fig. 18), conductivity shows a rather slight variation about a mean value of 2.2 mho.m^{-1} and between two extremes represented, under formulas (4) and (5) ($\log \Lambda$ is barely responsive to n_e and T_e variations), by the upper and lower limits of electron temperature, i.e. 21000°K and $13\,000^\circ\text{K}$, respectively. σ was only defined to a multiplication factor standing for the useful surface of the Rogovski probe used; however, the systematic error thereby introduced into the determination of

T_e in no case exceeds 20 %.

b) Velocity stays within the range of from 2.5 to 5 km.sec⁻¹, and as predictable from the simplified theories, shows modulations in time (Fig. 19), of a frequency that seems to be twice as high as that of the exciting currents.

With ionization complete and the composition of the plasma dependent on its temperature alone, once the velocity and the flow rate of injected propulsive gas are known, a mean value can be computed for electron density. Thus, for a flow of 1.2 g. sec⁻¹, a mean exhaust velocity of 4 km and a mean temperature of 17 000°K (corresponding as seen in 3.2.3, to a proportion of 2/3 of A⁺ ions and of 1/3 of A⁺⁺ ions), the electron density was found to be $1.7 \cdot 10^{21} \text{ m}^{-3}$.

3.4 - Discussion

3.4.1 - Determination of ionization coefficient and of electron temperature and density

On the state of ionization it should be noted that even with the gas fully ionized in the vicinity of the electron-density maxima, the possible presence of a not negligible proportion of neutrals near the minima cannot be ruled out in the event of the electron density being heavily modulated. As a matter of fact, such presence, which may result from non-homogeneous ionization at the start, admits of being neither disproved nor confirmed by the diagnostic methods used.

It can safely be said at this stage that there is a good measure of agreement between the two respective sets of results from the direct and from the indirect methods of electron temperature measurement. In any case, any necessary approximations to be applied to one of the two methods can always be checked up on by resort to the other. In particular, spectrography bears out the assumption of full ionization, which makes for an appreciable simplification of Ohm's law. Similarly, with instantaneous conductivity varying by some 35 % under the conditions described in¹⁵, the corresponding temperature variations justify definition of a mean value, which enables Boltzmann's law to be applied.

Attention is lastly drawn to the consistency between the two sets of electron density values (of the order of 10^{21} m^{-3}) as obtained by direct and by indirect means.

3.4.2 - Velocity measurements

Here again, the respective results from the direct and the indirect techniques are well in keeping, the mean velocity values obtained lying between 2.5 and 4 km.sec⁻¹ in case of a marked time-lag, i.e. high counterpressure.

A reduction in the latter gives rise to a notable increase in ejection velocity; the direct method yielded higher values (approx. 6.5 to 9.5 km.sec⁻¹) in case of short delay times, which correspond more closely to the actual aerodynamic conditions of continuous operation.

3.4.3 - Interpretation of luminous phenomena

The spectrographic results have shown that what the light emission

involves, at any rate on the outside of the accelerator, are not radiative recombination processes, which would yield a continuous spectrum, but a virtually simultaneous excitation and de-excitation of the fully ionized gas, at least in the neighbourhood of the electron-density peaks. Accordingly, the strong luminosity modulation observed may derive from fluctuations of either electron density or electron temperature, though luminous intensity is particularly sensitive to those of the latter (cf. formula (1)). Since the propagation velocity of the light modulations greatly differs from the fluid velocity, their overriding cause lies in a temperature modulation prevailing over any modulations of density.

It should also be borne in mind that the assumption underlying the indirect method, namely, that σ , and hence T_e , are solely dependent on the relative electric field $E - \mu B$, is grounded on a disregard of the electron-pressure and thermal-inertia terms. This implies, by the same token, that T_e and σ vary in the same sense as E' . The form of Ohm's law used will now show that the modulations of current density and of temperature follow those of the relative electric field. In fact, the luminous processes and current density have been found to propagate at much the same mean velocity, which is of the order of 20 km. sec^{-1} , and their modulations to be strictly in phase, as demonstrated by the records made simultaneously under varying conditions of flow-rate, delay and charging voltage (Fig. 20).

This, then, leads up to conceiving of a wave of temperature dependent on the relative electric field and propagating at its velocity in the mass

of plasma, independently of the plasma velocity. Thus we are faced with the propagation of hot zones of increased excitation, in which the light arising out of de-excitation travels at the rate of the relative field.

3.4.4 - Form of Ohm's law

Ohm's law as relevant to this type of accelerator has been inquired into experimentally^{10, 15}, and by a theoretical approach¹⁰, which is summed up below on broad lines, together with its general results.

Some of the foregoing measurements have yielded approximate values for electron density and temperature, which help to simplify the motion and energy equations of a two-fluid (electrons and ions) model, by providing support for the following hypotheses :

- a) Full ionization of plasma
- b) Pressure terms negligible
- c) Energy exchange between electrons and ions (due to the difference in their respective temperatures) negligible .

By making the further assumption, a posteriori substantiated by the consistent results deriving from the indirect method, that the electrons possess a negligible thermal inertia, and also that there is no loss of energy through inelastic collisions (apart from the initial ionization process), a simplified electron energy equation is obtained; provided the temperature at the wall is low in comparison with the electron temperature in the centre of the channel, this leads to a straightforward relationship linking the latter to the half-height h of the channel and the relative electric field

$$(6) \quad T_e = 1,08 \cdot 10^4 h(E - uB)$$

Using (4) and (5), a simplified Ohm's law is obtained

$$(7) \quad j = 0,88 \cdot 10^4 \frac{h^{3/2}(E - uB)^{5/2}}{\text{Log } \Lambda}$$

The main advantage of this model is that it allows for the transport coefficients depending on electron temperature.

Another model¹⁶, this time introducing the terms of convection and of exchange, due to lack of thermal equilibrium between the different species (electrons, ions, atoms) has been treated numerically; the results do not run counter to the regime previously obtained, which appears to be an "asymptotic" one rapidly arrived at by the flow under suitably chosen initial conditions (temperatures, densities), and that even in case of an incompletely ionized plasma (for degrees of ionization over 0.1).

Formula (7) has thus been subjected to a series of experimental measurements.

As for the dependence of j on the $3/2$ power of the channel half-height h , it should be pointed out that there have been made comparative measurements on two accelerators of differing channel heights, working under similar dynamic and electromagnetic conditions. The general trend of results seems to bear out the suggested formula, and they tend to tally the more the higher the electric field at work.

The experimental values obtained for n_e and T_e suggest that $\log \Lambda$ is practically constant ($\text{Log } \Lambda = 7.05$ for $n_e = 10^{21} \text{ m}^{-3}$ and $T_e = 10^4 \text{ K}$).

Lastly, the variation of j as a function of $(E - uB)$ can be studied in the light of the measurements of j and E when B is zero. A close look at the way j shapes up as a function of E during one particular firing reveals that the tests are remarkably well repeatable (Fig. 21), and that there exists an empirical law of the type : $j \propto E^\alpha$ (8) which differs from the one adumbrated by the theoretical model ($\alpha = 1.14$ as relating to Fig. 21). This empirical formula solely depends on the initial charging voltage (fig. 22). Generalized into : $j \propto (E - uB)^\alpha$ (9) it yields fully coherent results in determining velocity by the use of the indirect method.

It appears accordingly that while formula (7) (which comes down to $j = 0.8 E_0^{5/2}$ in the test conditions covered by figure 21) gives an acceptable order of magnitude for current density within the range of medium-strength (approx. 500 V.m^{-1}) electric fields, it fails to cover its variation with the local electric field (Fig. 21). The most open to criticism amongst the basic hypotheses on the theoretical model governed by formula (7) concerns the losses by inelastic collisions. In particular, evaluation of the power radiated by the various spectral lines present yields an order of magnitude comparable with that of the Joule effect term j^2 / σ , which is indicative of the importance plasma radiation comes in for the energy balance. It should however be noted that by introducing a radiation term dependent on T_e into the electron energy equation, the basic assumption underlying the indirect method of plasma velocity determination, namely that T_e is

a function of the relative electric field ($E - \mu B$) alone, is not called in question.

CONCLUSION

The evolutive nature of the plasma throughout each discharge, an inherent feature of pulsed operation, has enabled the fundamental parameters of the plasma generated to be determined with the aid of the set-up under review, in spite of the influence of unwanted non-periodic parameters incident to this very mode of operation as a result of thermal and chemical inertia.

Following the first two periods of discharge covering the initial ionizing phase, definite magnetodynamic flow regimes have accordingly been observed within a plasma fit to be treated as fully ionized, of a medium density of approx. 10^{21} particles m^{-3} , medium temperature of around $20,000^\circ\text{K}$, medium velocity of between 3 and 9 $\text{km} \cdot \text{sec}^{-1}$ for a travelling field propagation velocity of some 20 km sec^{-1} in the region of the exit plane.

As regards the microscopic phenomena, it may be said that

- a) the full-ionization hypothesis seems to have proved its worth;
- b) the terms of pressure and of heat exchange between electrons and ions, disregarded in the initial model, leave the theoretical asymptotic regime of the plasma unaffected;
- c) Ohm's law as relevant to this theoretical regime cannot safely be said to apply but the experiment has demonstrated an empirical Ohm's law pertinent to the set-up and especially suitable for use in computing the actual performance of the device.

Special notice is due to the benefit accruing from the use of passive probes, which are gainfully applicable to any pulse-based apparatus, in the direct measurement of system parameters and in indirectly determining the basic characteristics of the plasma generated.

Lastly, it would seem that any improvement made in the theoretical model designed for an analysis of the phenomena brought into play after the initial ionizing phase must take account, in particular, of the inherent processes of radiation.

References

- ¹Moulin, Th., Paulon, J., and Defranould, Ph., "Mesure des performances d'un accélérateur à ondes progressives", 6th Symposium on Engineering Aspects of Magnetohydrodynamics, Pittsburg, 21-23 April 1965.
- ²Janes, G.S., "Magnetohydrodynamic propulsion", AVCO Research Report 90, August 1960.
- ³Penfold, A., "Travelling wave plasma accelerators", Preprint 2130-61, Am. Rocket Soc., 1961.
- ⁴Jones, R., and Palmer, R., "Travelling wave plasma engine program at NASA Lewis Research Center", 3rd Symposium on Engineering Aspects of Magnetohydrodynamics, Rochester, 28-29 March 1962.
- ⁵Moulin, Th., "Contribution à l'étude des accélérateurs de plasma à ondes progressives", XIVth International Astronautical Congress, Paris, 1963, Pergamon Press, Vol. 1, pp. 423-446.
- ⁶Fabri, J., Moulin, Th., Paulon, J., and Charpenel, M., "Sur le fonctionnement des accélérateurs de plasma à ondes progressives", C.R. Acad. Sc. Paris, v. 263 B, 1966, pp. 234-236.
- ⁷Griem, H.R., "Plasma spectroscopy", Mc Graw Hill, 1964, Chap. 6.
- ⁸Griem, H.R., "Plasma spectroscopy", Mc Graw Hill, 1964, p. 541.
- ⁹Sitt, B., "Analyse par photographie ultra-rapide d'un plasma accéléré par ondes progressives", Colloque National sur la Physique des Milieux ionisés, Grenoble, 25-26 May 1967, Journal de Physique, Suppl. au No.4, v. 29, April 68.

¹⁰Rager, J.P., "Accélérateur de plasma annulaire à ondes progressives. Etude du régime d'équilibre entre effet Joule et conduction thermique", Thèse 3ème cycle, Faculté des Sciences de Paris, 1967.

¹¹Fournier, G., Rager, J.P., and Sitt, B., "Mesure de la conductivité et de la vitesse d'un plasma dense accéléré par un champ électromagnétique moyenne fréquence", 2ème Colloque International sur les Interactions entre les Champs oscillants et les Plasmas, CEN Saclay, 15-18 January, 1968.

¹²Robert, E., and Reding, L., "Etude expérimentale d'un accélérateur de plasma à électrodes linéaires", Revue Générale de l'Electricité, v. 77, No.11, November 1968.

¹³Rager, J.P., and Sitt, B., "Etalonnage d'une bobine de Rogowski utilisée pour la mesure des densités de courant dans un accélérateur de plasma pulsé", Note Technique n° 14, 1018/E. (Unpublished Report).

¹⁴Spitzer, L., "Physique des gaz complètement ionisés", Monographie Dunod No. 9, 1959.

¹⁵Fournier, G., "Détermination, avec des moyens passifs, des paramètres fondamentaux de l'écoulement d'un plasma induit dans un canal annulaire, par un champ électromagnétique moyenne fréquence", La Recherche Aérospatiale, No.126, September-October 1968.

¹⁶Rager, J.P., Accélération électromagnétique d'un plasma. Comparaison des schémas à un et plusieurs fluides. Note Technique n° 15/1018/E. (Unpublished Report).

List of Captions

Figure 1 : ONERA travelling-wave accelerators.

Figure 2 : Schematic diagram of ONERA's travelling-wave accelerators,
together with relevant applied fields.

Figure 3 : Block diagram of set-up - Propulsive-gas supply.

Figure 4 : Curve of static pressure at injection P_k plotted vs. time.

Figure 5 : Static pressure at injection P_k plotted vs. tank pressure P_R .

Figure 6 : Relative flow rate \dot{m}/\dot{m}_{\max} plotted vs. delay.

Figure 7 : Line spectrum of argon plasma.

AI : neutral argon, AII : singly-ionized, A : unidentified
argon (probably AIII), Cd, Hg, K : standard lines uses for
calibration.

Figure 8 : Mean electron temperature diagram.

Figure 9 : Standard oscillogram of hyperfrequency (upper trace) and photo-
multiplier (lower trace) signals. Test conditions : Charging
voltage 14 kV, Tank pressure 1400 mmHg, Delay 2.1 ms.

a- Distance from exit plane 50 mm - Sweep rate : 5 μ sec/cm.

b- Distance from exit plane 200 mm, Sweep rate : 10 μ sec/cm.

Figure 10 : Combined results of plasma velocity measurements.

Tank pressure 1400 mmHg, Delay 2.1 ms, Charging voltage 14 kV.

Figure 11 : Combined results of plasma velocity measurements.

Tank pressure 1400 mmHg, Delay 2.1 ms, Charging voltage 12 kV.

Figure 12 : Combined results of plasma velocity measurements.

Tank pressure 300 mmHg, Delay 3.5 ms, Charging voltage 12 kV.

Figure 13: Combined results of plasma velocity measurements.

Tank pressure 300 mmHg, Delay 3.5 ms, Charging voltage 10 kV.

Figure 14: Block diagram of current density test circuit.

Figure 15 : Oscillograms of current density for various rates measured 15 mm from exit plane (identical scale).

Figure 16 : Max. current density plotted vs. mass flow rate at constant operating time. T_0 = first significant time (reference time).
 $T_j = T_0 + j \frac{T}{2}$ $j = 1, 2, \dots, 6$. T = energizing currents period.

Figure 17 : Mean propagation velocity of current density.

Tank pressure 1600mmHg, Delay 2.2. ms, Charging voltage 12 kV.

(The test points are marked with the number of the corresponding peak of j - cf. Fig. 15).

Figure 18 : Current density J as a function of the electric field E at instants of zero magnetic induction. Flow rate 1.4. gsec⁻¹.

Figure 19 : Plasma velocity plotted vs. time.

Flow rate 1.4 gsec⁻¹, Delay 3.5 ms, Charging voltage 10 kV.

The encircled points stand for $J = 0$. The instants when magnetic induction becomes zero are marked by t_0 .

Figure 20 : Standard oscillogram showing coincidence of luminous signal (upper trace) and current density (lower trace) modulations 5 mm downstream of exit plane. Sweep rate 5 μ sec/cm.

Figure 21 : Typical current-density curves plotted as a function of the electric field (linked-up points relate to one and the same firing). Charging voltage 10 kV. The test points are marked with the No of the corresponding zero of B .

Figure 22 : Determination of the empirical Ohm's law plotted vs. charging voltage.

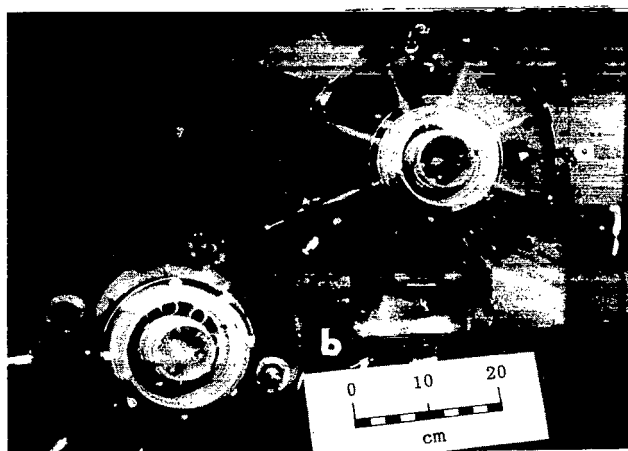


Figure 1

Figure 2

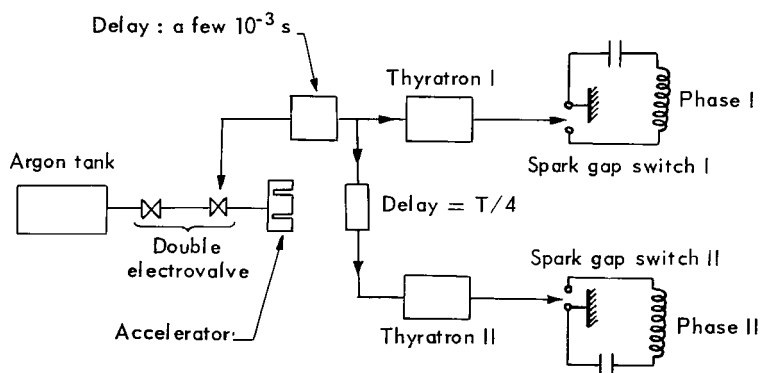
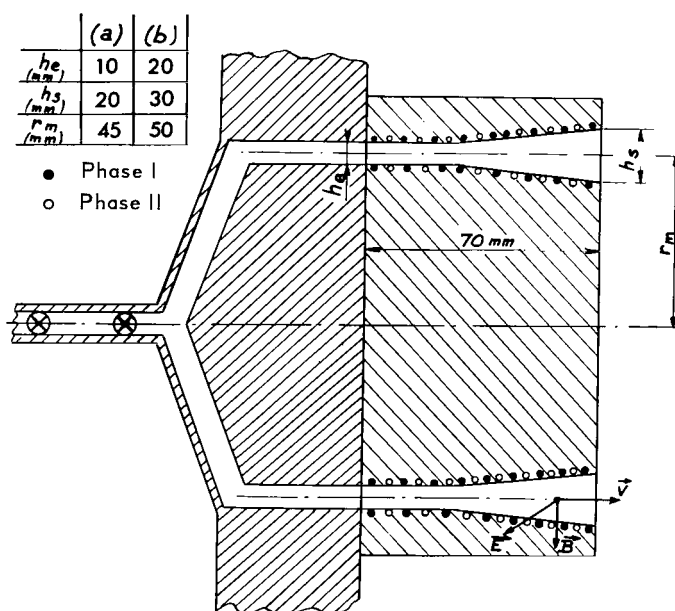


Figure 3

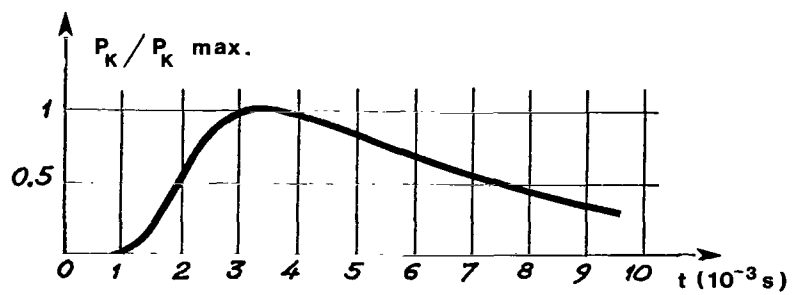


Figure 4

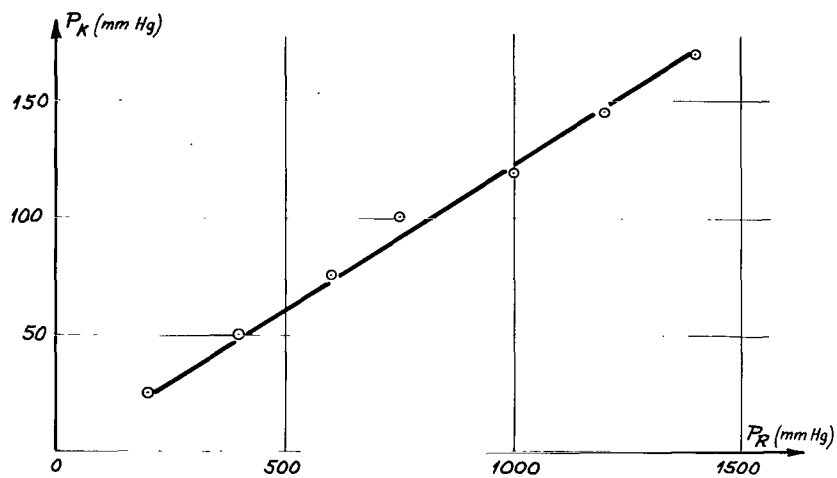


Figure 5

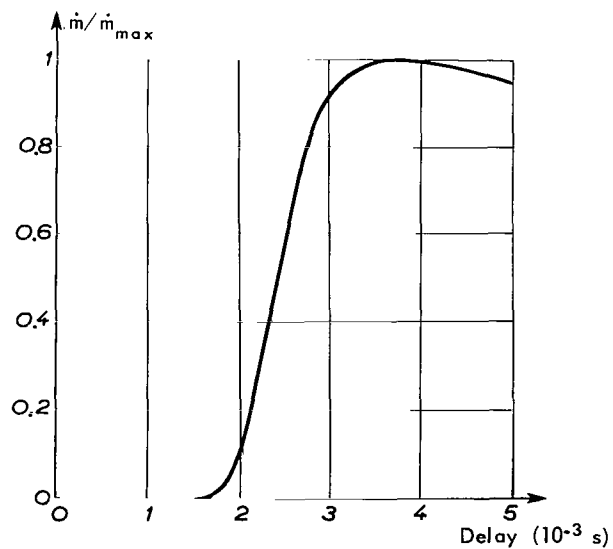


Figure 6

Figure 7b
- 34 -

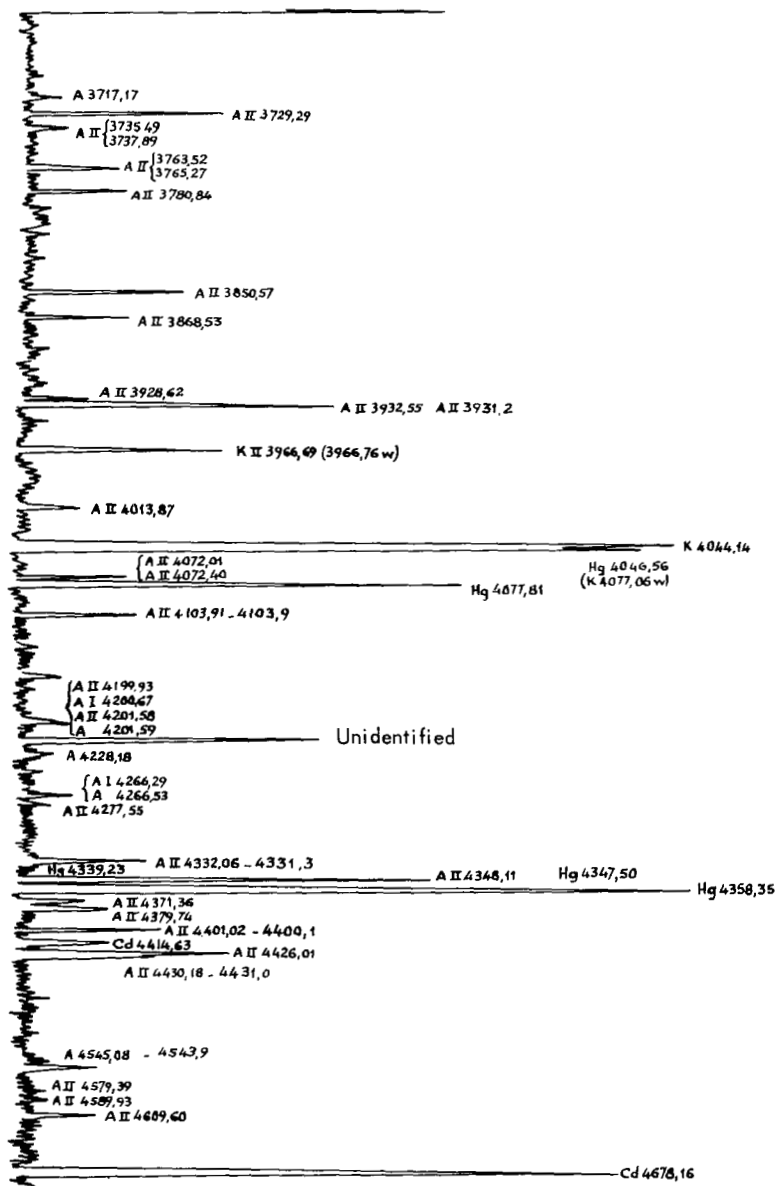
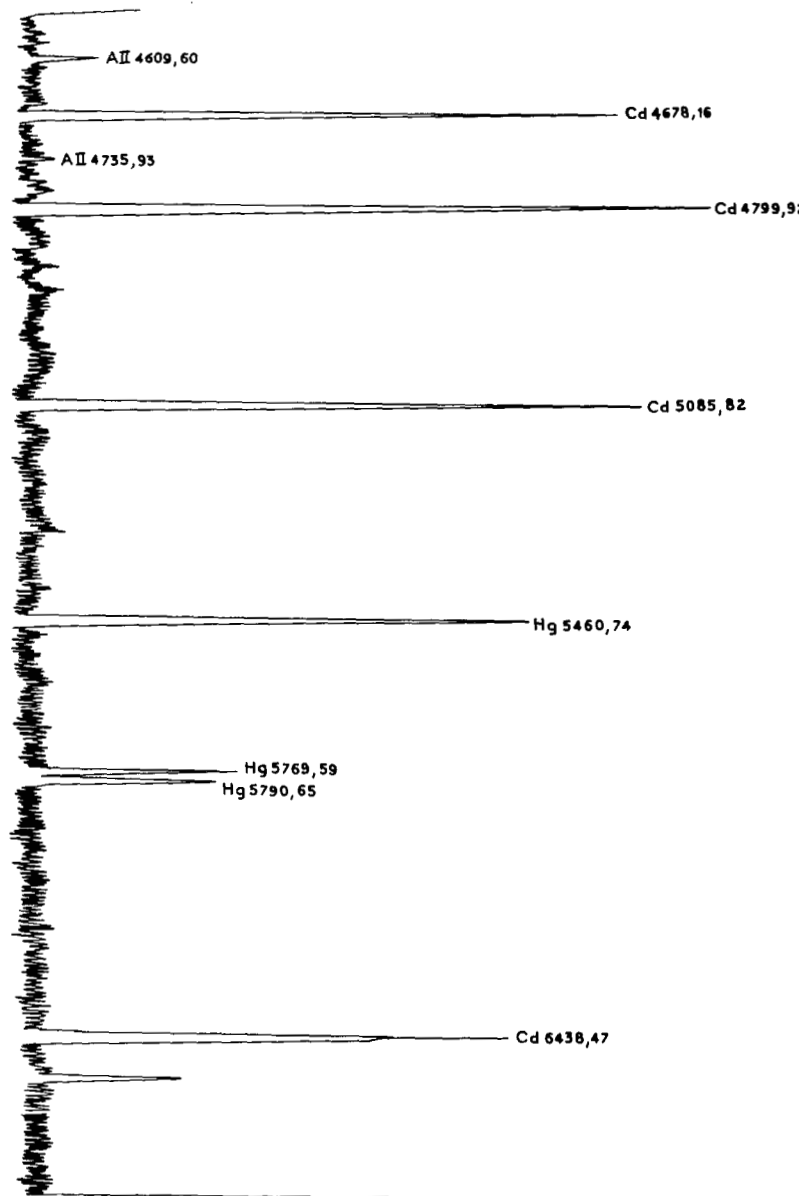


Figure 7a



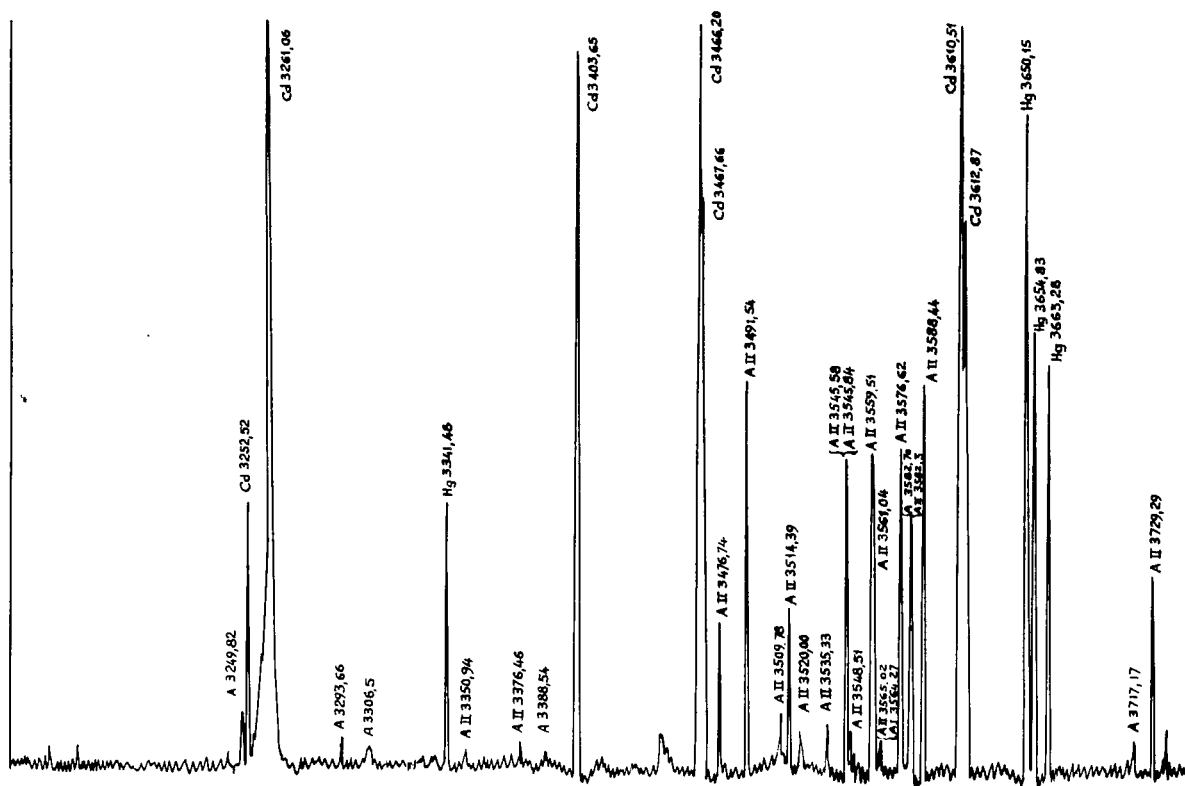


Figure 7c

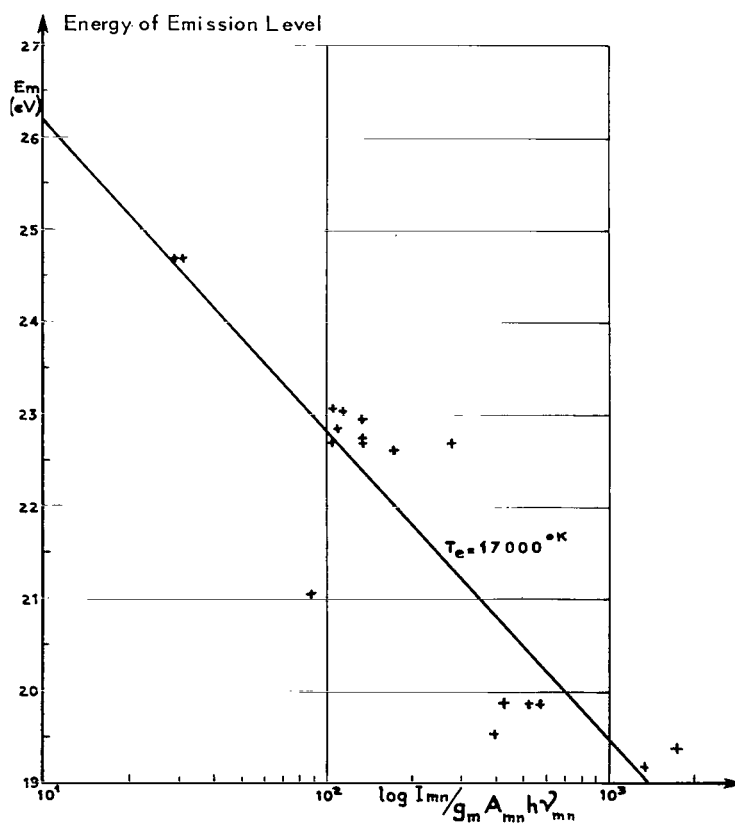


Figure 8

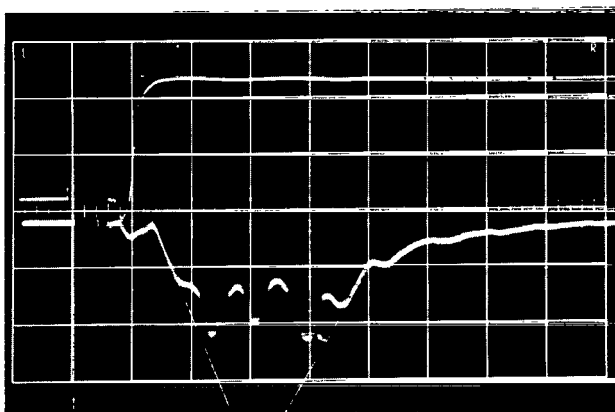


Figure 9a

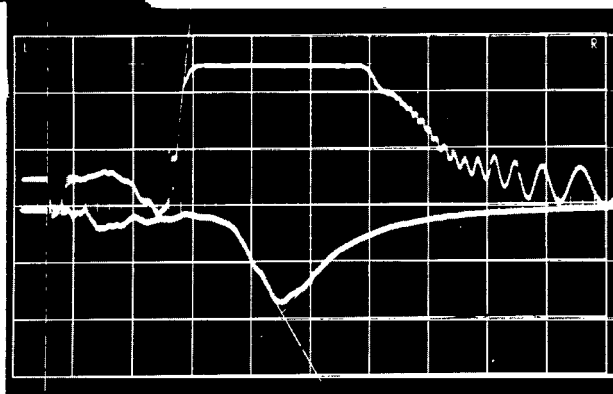


Figure 9b

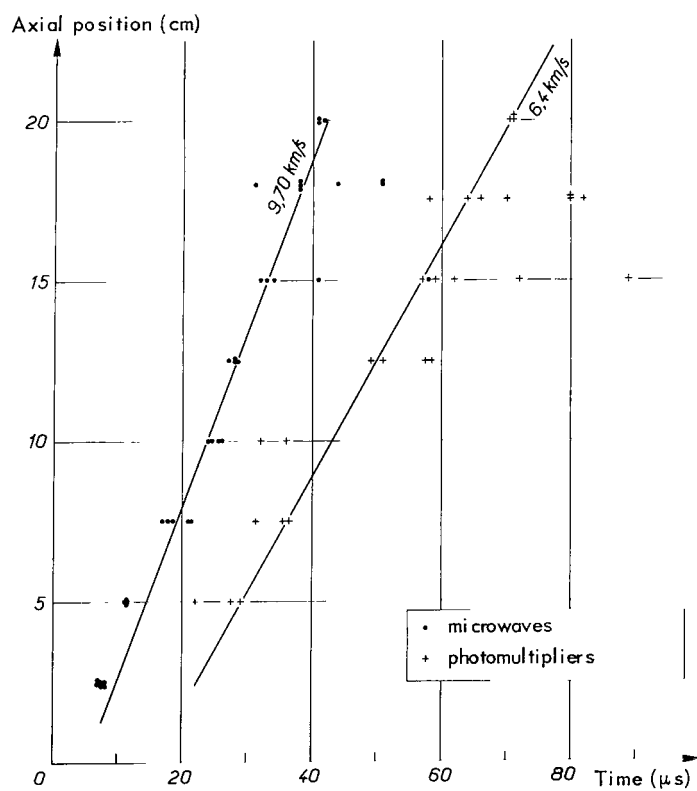


Figure 10

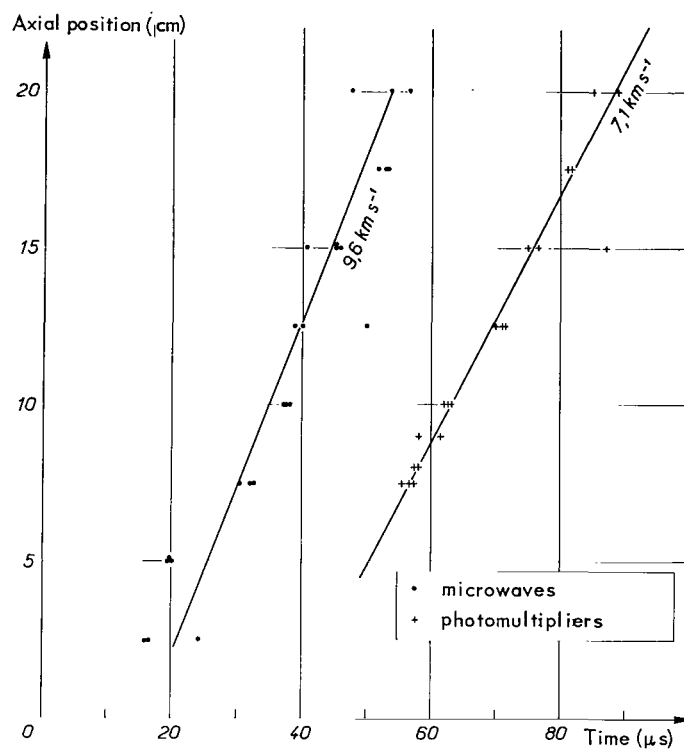


Figure 11

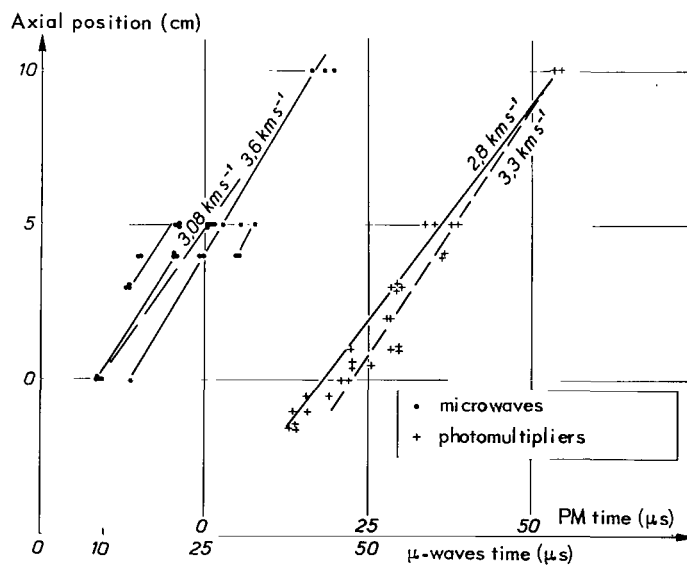


Figure 12

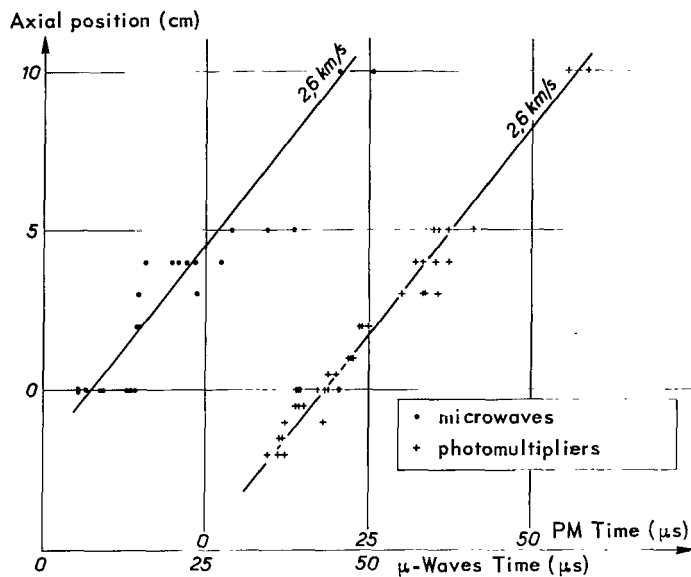


Figure 13

Figure 14

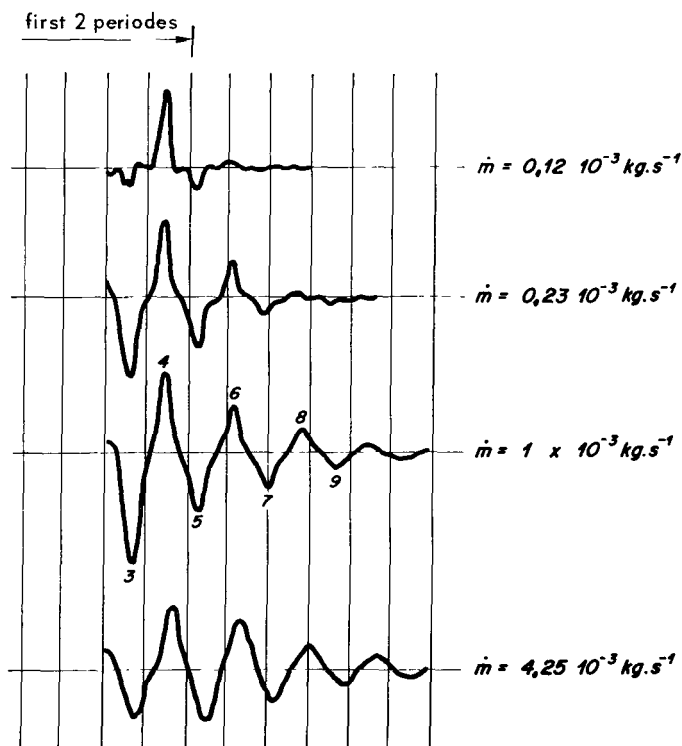
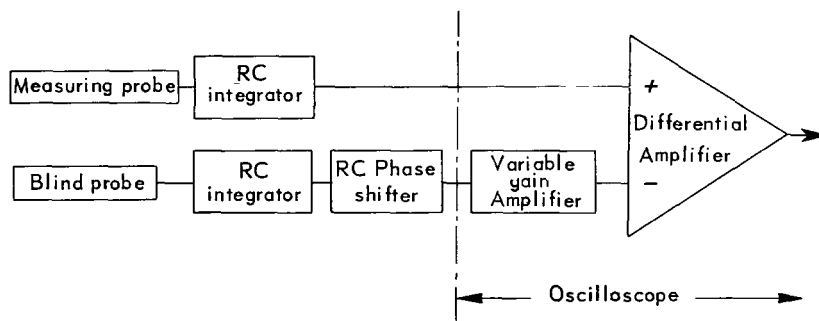


Figure 15

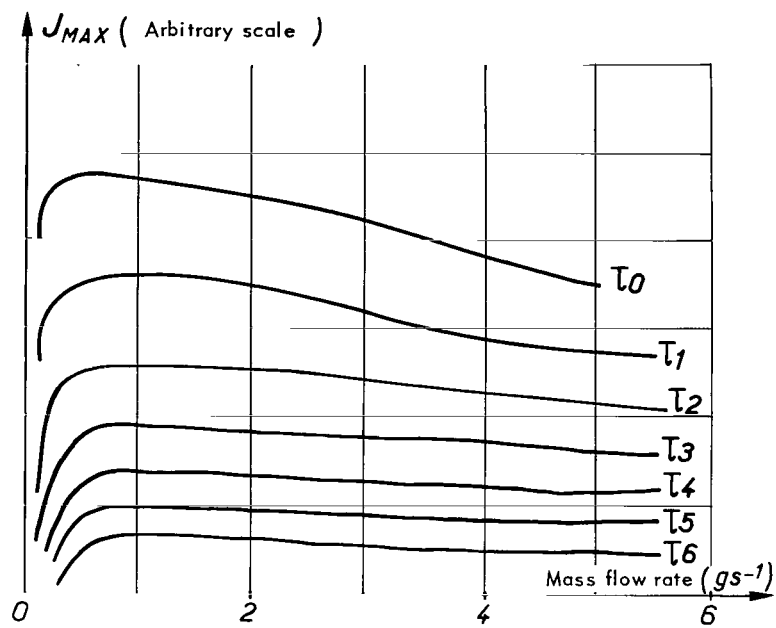


Figure 16

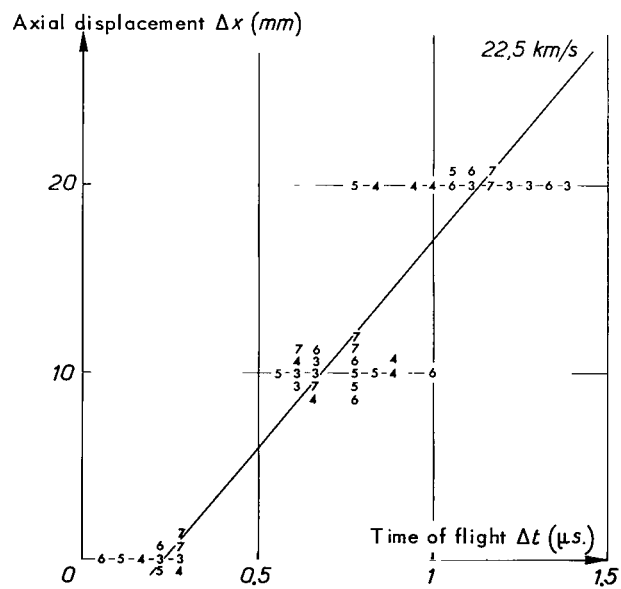


Figure 17

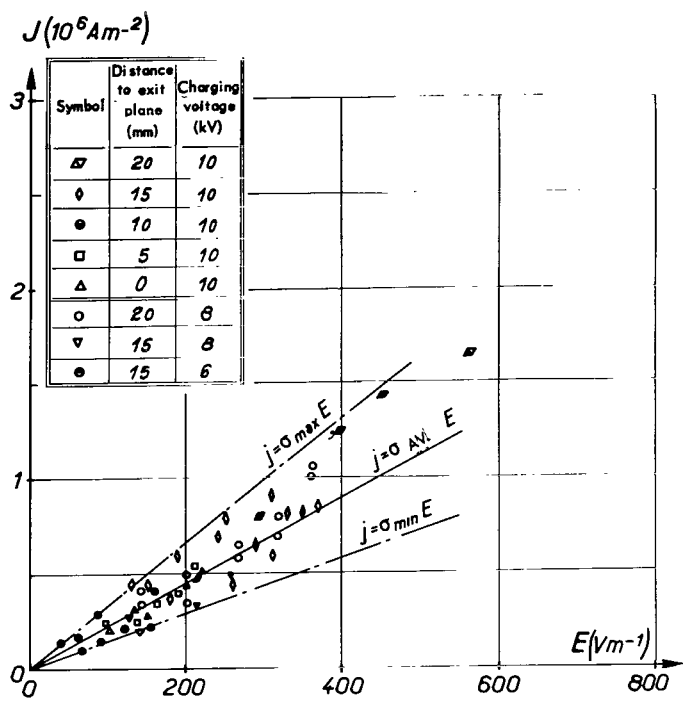


Figure 18

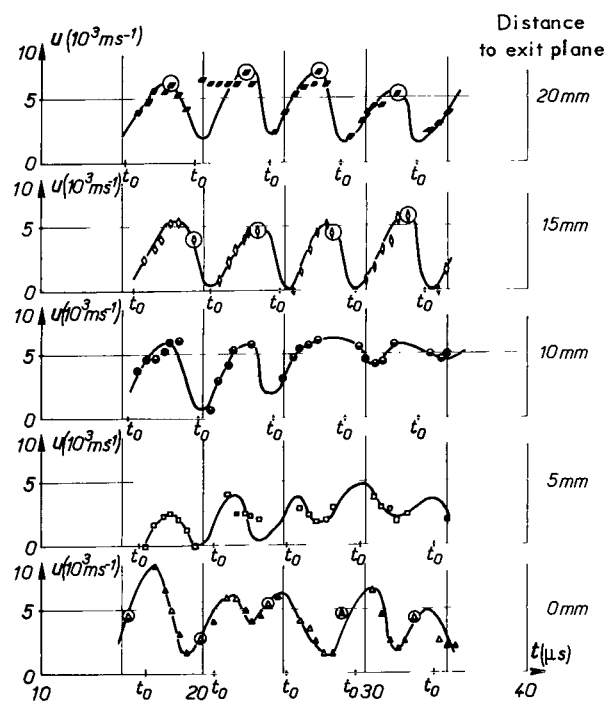


Figure 19

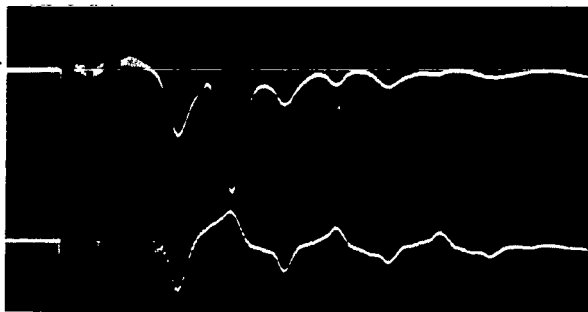


Figure 20

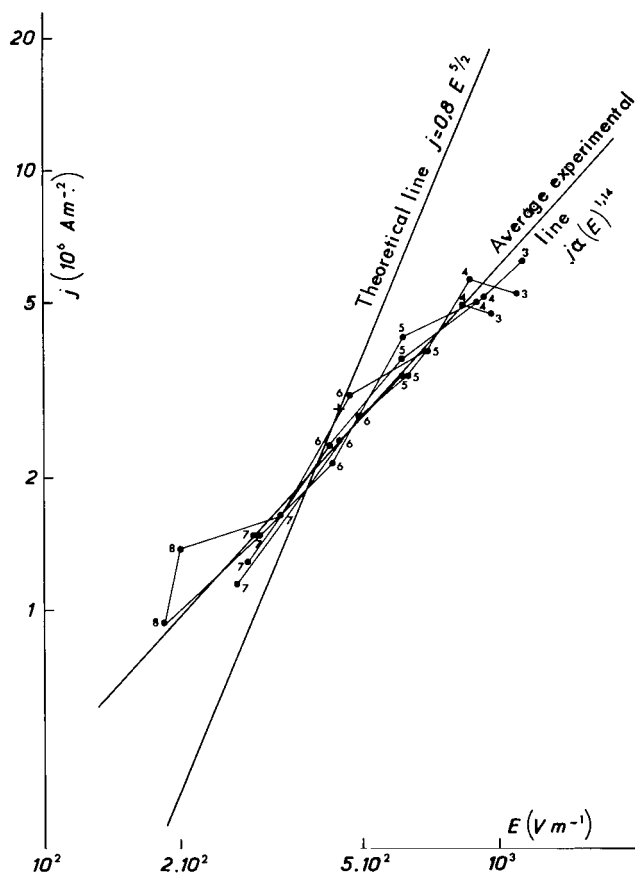


Figure 21

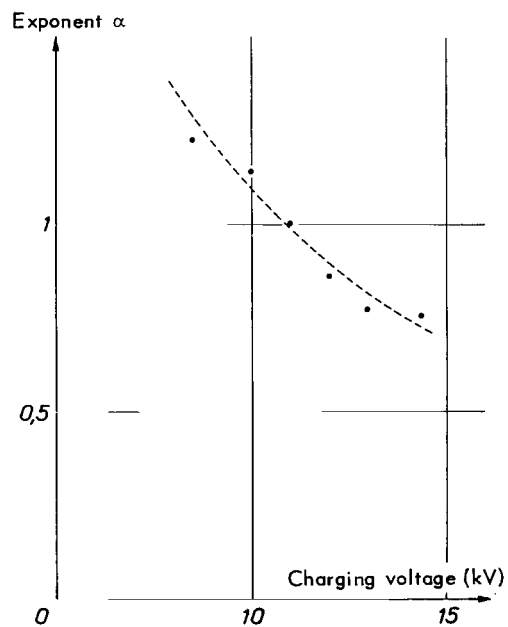


Figure 22

NATIONAL AERONAUTICS AND SPACE ADMINISTRATION

WASHINGTON, D. C. 20546

OFFICIAL BUSINESS

PENALTY FOR PRIVATE USE \$300

FIRST CLASS MAIL



POSTAGE AND FEES PAID
NATIONAL AERONAUTICS AND
SPACE ADMINISTRATION

025 001 C1 U 28 710903 S00903DS
DEPT OF THE AIR FORCE
AF SYSTEMS COMMAND
AF WEAPONS LAB (WL0L)
ATTN: E LOU BOWMAN, CHIEF TECH LIBRARY
KIRTLAND AFB NM 87117

POSTMASTER: If Undeliverable (Section 158
Postal Manual) Do Not Return

"The aeronautical and space activities of the United States shall be conducted so as to contribute . . . to the expansion of human knowledge of phenomena in the atmosphere and space. The Administration shall provide for the widest practicable and appropriate dissemination of information concerning its activities and the results thereof."

— NATIONAL AERONAUTICS AND SPACE ACT OF 1958

NASA SCIENTIFIC AND TECHNICAL PUBLICATIONS

TECHNICAL REPORTS: Scientific and technical information considered important, complete, and a lasting contribution to existing knowledge.

TECHNICAL NOTES: Information less broad in scope but nevertheless of importance as a contribution to existing knowledge.

TECHNICAL MEMORANDUMS: Information receiving limited distribution because of preliminary data, security classification, or other reasons.

CONTRACTOR REPORTS: Scientific and technical information generated under a NASA contract or grant and considered an important contribution to existing knowledge.

TECHNICAL TRANSLATIONS: Information published in a foreign language considered to merit NASA distribution in English.

SPECIAL PUBLICATIONS: Information derived from or of value to NASA activities. Publications include conference proceedings, monographs, data compilations, handbooks, sourcebooks, and special bibliographies.

TECHNOLOGY UTILIZATION PUBLICATIONS: Information on technology used by NASA that may be of particular interest in commercial and other non-aerospace applications. Publications include Tech Briefs, Technology Utilization Reports and Technology Surveys.

Details on the availability of these publications may be obtained from:

SCIENTIFIC AND TECHNICAL INFORMATION OFFICE

NATIONAL AERONAUTICS AND SPACE ADMINISTRATION

Washington, D.C. 20546